Analyst

Accepted Manuscript

ROYAL SOCIETY OF CHEMISTRY

www.rsc.org/analyst

Cite this: DOI: 10.1039/c0xx00000x

www.rsc.org/xxxxxx

ARTICLE TYPE

Electrochemiluminescence Resonance Energy Transfer between Graphene Quantum Dots and Gold Nanoparticles for DNA Damage Detection

Qian Lu,[a] Wei Wei,[a] Zhenxian Zhou,[b] Zhixin Zhou,[a] Yuanjian Zhang,[a] Songqin Liu*[a]

Received (in XXX, XXX) Xth XXXXXXXXX 20XX, Accepted Xth XXXXXXXXX 20XX
DOI: 10.1039/b000000x

A bright blue luminescent graphene quantum dots (GQDs) with major graphitic structured nanocrystals and photoluminescence (PL) quantum yield of 15.5% was synthesized and used for monitoring of DNA damage. The GQDs was prepared by ultraviolet irradiation without using chemical agent. The as-prepared GQDs showed excitation-dependently PL and stable electrochemiluminescence (ECL) behavior. The AuNPs were firstly linked with capturing single-stranded DNA (cp53 ssDNA) to form AuNPs-ssDNA. The ECL signal of GQDs could be quenched by non-covalent binding of AuNPs-ssDNA to GQDs due to the occurrence of the electrochemiluminescence resonance energy transfer between GQDs and AuNPs. When AuNPs-ssDNA was hybridized with target p53 DNA to form AuNPs-dsDNA, the non-covalent interaction between GQDs and ds-DNA weakened and the ECL of GQDs recovered. This engendered an ECL sensor for detection of target p53 ssDNA with a detection limit of 13 nM. The resultant ECL sensor could be used for DNA damage detection based on the different bonding ability between damaged target p53 ssDNA to cp53 ssDNA linked AuNPs. The presented method could be expanded in the development of other ECL biosensors for quantification of nucleic, single nucleotide polymorphism or other aptamer-specific biomolecules.

1. Introduction

Recently, carbon nanostructured materials received considerable attention for their promising applications in supercapacitors,[1] fuel cell,[2] and biosensor. These carbon nanostructured materials include carbon nanotubes,[3-5] carbon nanofibers,[6-8] carbon nanocapsules,[9,10] carbon dots and graphene.[11-14] It has been demonstrated that the cleaving of graphene nanosheets into graphene quantum dots (<10 nm) may increase their photoluminescence[15-21] due to their remarkable edge effects and strong quantum confinement effect. GQDs have some diverting advantages, such as low cytotoxicity, good biocompatibility, excellent solubility and stable photoluminescence. These advantages made them promising in photovoltaic device,[22] bioimaging,[20] biosensing and drug delivery.[18,23,24] Synthesis of GQDs generally has two ways: bottom-up and top-down.[17,25,26] As for the top-down strategy, the large graphene oxide (GO) nanosheets were cleaved into smaller sheets by oxidation process.[15-21] Then, in alkaline solution, GO sheets could be easily reduced by hydrothermal or UV-*vis* irradiation. For example, Zhang et al. prepared GQDs by a photo-fenton reaction for construction of a novel DNA cleavage system. The photo-Fenton reaction was initiated by exposing the mixture of oxidized graphene, H_2O_2, and $FeCl_3$ to an irradiation lamp.[23] By heating of oxidized graphene solution in DMF at 200 ºC for 5 h, GQDs were obtained with one-step solvothermal method. The resultant GQDs with strongly green-photoluminescent and low cytotoxicity were successfully applied for bioimaging.[18] Ajayan and co-workers derived GQDs for high contract bioimaging by chemical oxidation and cutting of micrometer-sized pitch-based carbon fibers in a mixture of concentrated H_2SO_4 and HNO_3 for 24 h.[21] With the assistance of microwave irradiation, Zhu et al. synthesized two-color GQDs by reducing the oxidation time of GO nanosheets in the concentrated mixture solution of HNO_3 and H_2SO_4 to 1-5 h. Those GQDs have stabilized ECL performance and were applied for detection of Cd^{2+}.[17]

In the present work, a facile approach for preparation of GQDs was proposed by combining of thermal reduction and cleaving in an oxidation procedure as well as UV-light irradiation reduction. Compared with the previously reported methods [17,18,21,23,24] which used either hydrothermal reaction or ultraviolet radiation, our approach could greatly shorten the reaction time and reduce the use of chemical reagents. Moreover, the

electrochemiluminescence resonance energy transfer (ERET) between GQDs and AuNPs (Scheme 1), so as to realize the dynamic quenching of ECL signal, was observed. To the best of our knowledge, this is the first report of the ERET between GQDs and AuNPs, and it opens new opportunities for sensitive detection of biorecognition events.

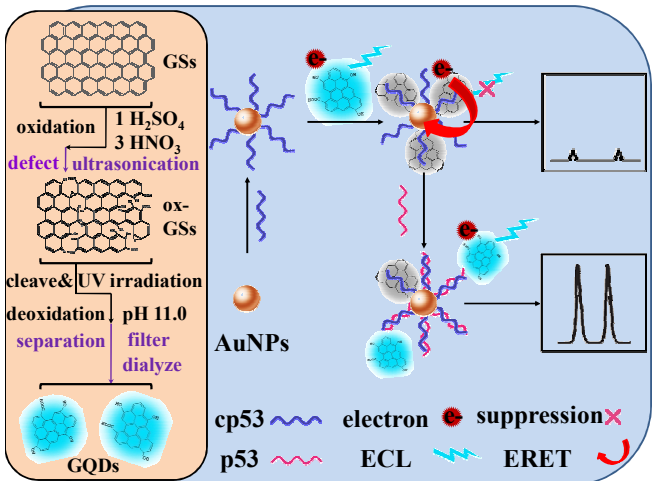

Scheme 1. Schematic representation of preparation of GQDs and biosensing mechanism by AuNPs induced ECL quenching of GQDs.

2. Experimental

2.1 Reagents.

The styrene-7,8-oxide (SO), phenylglyoxylic acids (PGA) and mandelic acids (MA) were obtained from Sigma-Aldrich. Tris-(2-carboxyethyl) phosphine hydrochloride (TCEP) was provided by thermo scientific (USA). All other chemicals and solvents were of analytical grade. Colloidal gold nanoparticles (AuNPs) with diameter of approximately 13 nm (Fig. S1 right) were prepared by the citrate reduction of $HAuCl_4$ according to previous reports.[27-29] TEM image showed that the AuNPs had an average diameter of 13 nm (Figure S1). The presence of characteristic surface plasmon resonance band at approximately 522 nm in the UV-vis spectrum (Figure S1, curve a) confirmed the formation of spheroid AuNPs by this method.[30]

All the oligonucleotides were synthesized and depurated using high-performance liquid chromatography by Sangon Biological Engineering Technology & Co. Ltd. (Shanghai, China). The sequences were as follows:

Capture DNA: 5'-SH-C6 GG CAC AAA CAC GCA CCT CAA -3'

Target p53 DNA: 5'-TTG AGG TGC GTG TTT GTG CC -3'

Single-base mismatch p53 DNA: 5'-TTG AGG TGC GAG TTT GTG CC-3'

Three-base mismatch p53 DNA: 5'-TTG AGG TGC CAC TTT GTG CC-3'

TNF-α sequence: 5'-CAA GAC CAC CAC TTC GAA ACC-3'

MUC1 aptamer sequence: 5'-GCA GTT GAT CCT TTG GAT ACC CTG G-3'

zDNA: 5'-ACA GGA TCG AAG GGG TAA CGT CAA GTC GCA-3'

The oligonucleotides were stored in phosphate buffer solution (PBS, 137 mM NaCl, 2.7 mM KCl, 10 mM Na_2HPO_4, and 2.0 mM KH_2PO_4, concentrated hydrochloric acid to adjust pH 7.4). Prior to use, the oligonucleotide samples were centrifuged at 5000 rpm for 5 min.

2.2 Instruments.

TEM images were performed on a JEM-2100 (JEOL, Japan) electron microscope operating at 200 kV. The ultraviolet-visible (UV-*vis*) absorption spectra were recorded with a 2450 UV-visible spectrophotometer (SHIMADZU, Japan). Fourier transform infrared spectroscopy (FT-IR) was recorded with a Model Tensor 27 instrument (Bruker, Germany). Raman spectra were collected using a DXR Raman microscope (λ_{exc}=532 nm, Thermo Fisher Scientific Inc., USA). Fluorescence spectra were obtained at room temperature with FluoroMax-4 spectrofluorometer (Horiba, Japan). Atomic force microscopy (AFM) images were obtained on an Agilent 5500 atomic force microscope (Agilent, USA).

Electrochemiluminescence (ECL) measurements were carried out on a MPI-E multifunctional electrochemiluminescent analytical system (Xi'an Remex Analyze Instrument Co., Ltd., China). 2 mL of PBS buffer (0.1 M, pH=7.4) containing 0.1 M $K_2S_2O_8$ was used as the electrolyte in ECL analysis. All ECL measurements were performed in a 5-mL glass cell. The electrode system was comprised of a platinum wire auxiliary electrode, an Ag/ AgCl (3 M KCl) reference electrode, and an Au working electrode. The potential range applied to the working electrode was between 0.75 V and -1.6 V, and the scan rate was 100 mV/s. The emission of the photomultiplier tube was biased at 800 V.

2.3 Synthesis of graphene quantum dots (GQDs).

The graphene quantum dots were prepared from graphite oxide according to previous reports with some modifications.[15,31,32] Firstly, 100.0 mg graphite oxide were dispersed in 1000 mL of deionized water and oscillated ultrasonically (150 W, 40 kHz) for 2 h. The mixture was centrifuged at 3000 rpm for 30 min to collect graphene oxide.[30] The resultant graphene oxide was dried and thermally deoxidized in a tube furnace at 300 °C for 2 h, yielded the silver gray metallic luster of graphene sheets (GSs).[15] Secondly, 80.0 mg of as-prepared graphene sheets was oxidized in the mixture of concentrated H_2SO_4 (16 mL) and HNO_3 (48 mL) for 2 h under ultrasonication (150 W, 40 kHz). During this oxidation-ultrasonication process, the large graphene sheets could form defects which serve as reduction reactive sites, and were cleaved into small pieces. After that, the mixture was diluted with deionized water and filtered through a 0.22 μm microporous membrane to collect graphene oxide (ox-GSs ~ 68.0 mg). Thirdly, the resultant oxidized graphene was redispersed in 14 mL of deionized water, adjusted pH value with NaOH to 11.0, and treated with UV irradiation (254 nm, 150 W, height 3 cm) for 10 h. Then, the obtained black suspension was filtered through a 0.22 μm microporous membrane to separate out a brown filter liquid, which was further dialyzed in a dialysis bag overnight to culture graphene quantum dots.

2.4 Linkage of the capturing DNA to gold nanoparticles.

TCEP (100 mM) was freshly prepared in Tris buffer (20 mM, pH 7.3). 100 μL of 0.5 mM capturing DNA was mixed with 10 μL of freshly prepared TCEP at room temperature for 1 h. The excessive TCEP was removed from capturing DNA solution by using ultrafiltration centrifuge tube (~3000 NMWL) at 14000 rcf for 20 min. The activated capturing DNA was added to 2.5 mL of colloidal gold nanoparticles solution and allowed to react at room temperature for 16 h. The mixture solution was brought to PBS (10 mM, pH 7.0) containing NaCl (0.1 M) and kept in dark for 40 h. The capturing DNA linked gold nanoparticles were collected by centrifugation at 16100 rcf for 20 min, washed with deionized water twice, redispersed in 2.5 mL of PBS (0.1 M, pH 7.4) and kept in dark at 4 °C.[27,28] After the capturing DNA linked, the surface plasmon band of gold nanoparticles slightly shifted from 522.0 to 524.5 nm (Figure S1). This indicated a perturbation of the electrical double layer presented around the AuNPs on the addition of capturing DNA and confirmed the attachment of capturing DNA onto the AuNPs.[29,33]

2.5 DNA damaging by chemicals and DNA hybridization.

For DNA damaging measurement, target p53 DNA was incubated with damaging agents, such as SO, PGA, MA, sodium arsenite, toluene, ether, acetone, methanal, ethanal, methanol and ethanol for 1 h. The excessive damaging agents were removed from target p53 DNA solution by using ultrafiltration centrifuge tube (~3000 NMWL) at 14000 rcf for 20 min. Under the same conditions, the single-base mismatch and three-base mismatch of target p53 DNA were detected respectively.

The AuNPs-ssDNA and GQDs were incubated 30 min at room temperature. And then the hybridization of the AuNPs-ssDNA/GQDs with the target p53 DNA or damaged target p53 DNA needed 60 min at 37 °C.

3. Results and discussion

3.1 Synthesis and Characterization of GQDs.

The graphene obtained by thermal reduction of graphene oxide sheets could be cleaved into small pieces in the oxidation-ultrasonication process with concentrated H_2SO_4 and HNO_3. During the oxidation, oxygen-containing functional groups, eg., C-O-C, C=O, -OH and –COOH were introduced at the edge and on the basal plane, which were confirmed by the Fourier transform infrared (FT-IR) spectra (Figure S2, curve a and b), suggesting the successfully conversion from the reduced graphene to graphene oxide (ox-GSs).

The presence of these oxygen-containing groups led the resultant graphene oxide to be dispersible in water. After further UV-*vis* irradiation, the FT-IR spectrum of GQDs showed that the vibrational absorption band of C=O and -COOH at 1718 cm^{-1} and vibration band of C-O-C at 1059 cm^{-1} disappeared (Fig. S2, curve c), suggested that the graphene oxide sheets were reduced to GQDs by UV-*vis* irradiation process. Raman spectrum showed that the relative intensity ratio of the "disorder" D-band at 1355 cm^{-1} and the crystalline G-band at 1575 cm^{-1} for the as-prepared GQDs was 1.19 (Figure S3), which was very close to 1.26 by using hydrothermal route for cutting graphene sheets into blue-luminescent graphene quantum dots.[15]

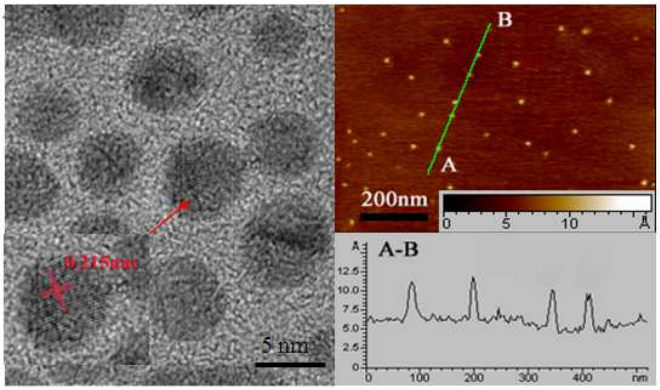

Figure 1. HRTEM image of GQDs (left). Inset: a representative image of individual GQDs. AFM image of GQDs and its corresponding height profile (right).

TEM images showed that the as-prepared GQDs had an average diameter of 4 nm (varied from 2 to 6 nm) and a lattice parameter of 0.215 nm (Figure 1 left), which was very close to previous report,[16-18] confirming the successfully synthesis of high crystallized GQDs. The AFM image showed that the topographic height of GQDs was mostly between 0.4 and 0.5 nm (Figure 1 right), suggesting that most of GQDs were single layered.[34] All these observations confirmed the thermal reduction of graphene to graphene oxide small pieces, and UV irradiation reduction of graphene oxide small pieces to GQDs.

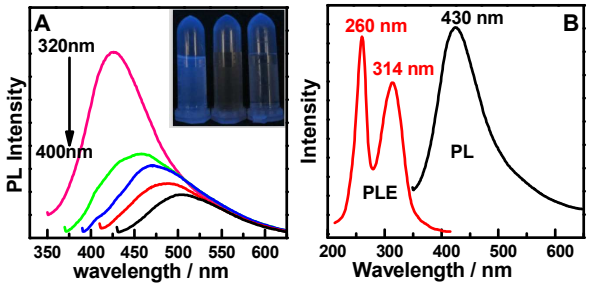

Figure 2. (A) PL spectra of GQDs at 320, 340, 360, 380, 400 nm excitation wavelengths. Inset: Photograph of GQDs, re-GSs, and oxidized graphene (from left to light) taken under 365 nm ultraviolet lamp. (B) Photoluminescence excitation spectrum (PLE) spectra of GQDs.

The as-prepared GQDs displayed a strong absorption peak at ca. 265 nm corresponding to the typical π-π* transition of aromatic sp^2 domains and a new absorption band at around 320 nm reflecting to the large edge effect of the ultrafine GQDs (Figure S4).[35] The as-prepared GQDs emitted bright blue luminescence excited by 365 nm ultraviolet lamp (Inset in Figure 2A) and had a PL quantum yield of ~15.5% in 320 nm. The PL spectrum of GQDs showed a largest peak at 430 nm with an excitation wavelength of 320 nm. When the excitation wavelength changed from 320 to 400 nm, the PL peak shifted to longer wavelengths with the intensity reducing quickly, showing an excitation-dependent PL feature (Figure 2A).[15-17] Further, GQDs showed only 16.1% changes in the PL intensity even after continuous exposure to a xenon arc-lamp (150 w) for 5 h (Figure S5). The photoluminescence excitation spectrum (PLE) on the

wavelength of 430 nm displayed two sharp peaks at 260 and 314 nm (Figure 2B). The 260 nm PLE peak was corresponded to the 265 nm absorption band due to the π-π* transition, whereas the 314 nm PLE peak was corresponded to the 320 nm absorption band due to the edge effect.

3.2 ECL of GQDs and ERET between GQDs and Au NPs.

3.2.1 ECL examination.

The GQDs exhibited good ECL activity in pH 7.4 PBS with $K_2S_2O_8$ as co-reactant. As shown in Figure 3A, when the potential was cycled negatively between 0.75 and −1.6 V, no ECL signal was observed in PBS buffer, and only a negligible ECL was obtained in PBS buffer containing $K_2S_2O_8$. However, when GQDs was added to $K_2S_2O_8$ containing solution, a strong ECL emission at −1.52 V that was about 18.2 times higher than background signal was observed. Obviously, the enhanced ECL signal was attributed to the ECL behavior of GQDs. In addition, negligible ECL signal was found in GQDs containing solution in the absence of $K_2S_2O_8$ and the ECL intensity of GQDs increased with the concentration of $K_2S_2O_8$ increasing (Figure S6), manifesting the important role of $K_2S_2O_8$ co-reactant. The ECL signal of GQDs was very stable with relative standard deviation of 1.63% upon continuous cyclic scans for 10 minutes (Figure S7).

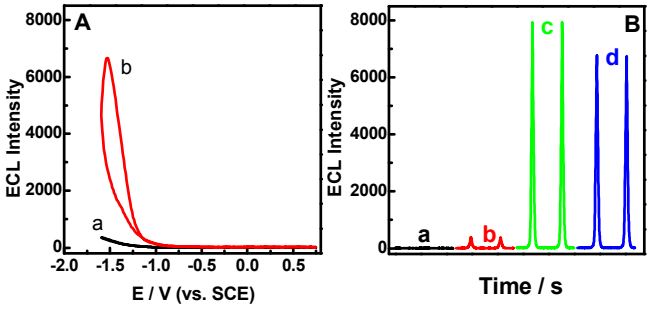

Figure 3. (A) ECL-potential curves of (a) 0.1 M pH 7.4 PBS buffer containing 0.1 M $K_2S_2O_8$ and (b) by addition of 10 μg/mL GQDs to (a). (B) ECL response of (a) 0.1 M pH 7.4 PBS, (b) 0.1 M pH 7.4 PBS+ 0.1 M $K_2S_2O_8$, (c) 0.1 M pH 7.4 PBS +0.1 M $K_2S_2O_8$+10 μg/mL GQDs with dissolved oxygen and (d) after removing dissolved oxygen with pure nitrogen for 20 min.

Previous report indicated that the ECL behaviors of GQDs were similar to that of CdTe,[36] CdSe/ZnSe[37,38] quantum dots and carbon,[39-41] or/and Si nanocrystals.[42] The considerable ECL mechanism of the GQDs was believed to form the excited-state GQDs* with the help of co-reactant $K_2S_2O_8$. The ground-state GQDs and co-reactant $S_2O_8^{2-}$ were first electrochemical reduced to the negatively charged $GQDs^{\bullet-}$ and $SO_4^{\bullet-}$ radicals. Then, strong oxidizing $SO_4^{\bullet-}$ radicals could react with $GQDs^{\bullet-}$ via electron-transfer annihilation, producing an excited state GQDs* that finally emitted light and came back to ground-state GQDs.[17,40] Moreover, when dissolved oxygen was removed from the solution by bubbling high-purity nitrogen, the ECL emission was lower than that of the air-saturated solution (Figure 3B). This identified that oxygen could be used to catalyze ECL emission of GQDs.[43,44] The whole ECL mechanism of GQDs could be described as following:

$$GQDs + e^{-} \rightarrow GQDs^{\bullet-}$$
$$S_2O_8^{2-} + e^{-} \rightarrow S_2O_8^{\bullet 2-}$$
$$S_2O_8^{\bullet 2-} \rightarrow SO_4^{2-} + SO_4^{\bullet-}$$
$$GQDs^{\bullet-} + SO_4^{\bullet-} \rightarrow GQDs^{*} + SO_4^{2-}$$
$$GQDs^{*} \rightarrow GQDs + h\nu$$

3.2.2 ERET Between GQDs and AuNPs.

When the capturing DNA (cp53 ssDNA) linked gold nanoparticles (AuNPs-ssDNA) was added to ECL system of GQDs, the strong non-covalent interaction between the single-stranded DNA and GQDs made AuNPs-ssDNA close to GQDs, which produced ECL quenching of GQDs (Fig. 4A). This ECL quenching could be ascribed to the energy transfer from the GQD to the AuNPs, which is similar to the case of the fluorescence quenching of quantum dots by the corresponding nanoparticles.[45,46] The kinetics of these processes should follow the Stem-Volmer quation:

$$I_0 / I = 1 + K_q c_q$$

Where I_0 is the intensity of ECL without a quencher, I is the intensity of ECL with a quencher, K_q is the ECL quenching rate coefficient, and c_q is the concentration of the quencher.[47,48] In our case, the plot of I/I_0 vs. the concentration of AuNPs-ssDNA showed a linear relationship (inset in Figure 4A). Therefore, it demonstrated that the ECL signal of GQDs querching by AuNPs-ssDNA had followed the Stern–Volmer equation and was the dynamic quenching process.

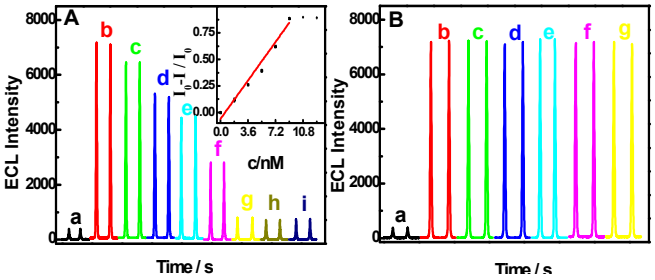

Figure 4. (A) ECL emission spectra of PBS buffer (100 mM, pH=7.4) solution containing 0.1 M $K_2S_2O_8$ (a). ECL emission spectra of GQDs (10 μg/mL) at AuNPs-ssDNA concentration of 0, 1.8, 3.6, 5.4, 7.2, 9.0, 10.8, and 12.6 nM (b-i). Inset in A: ECL intensity ratio of GQDs upon addition different amount of AuNPs-ssDNA. (B) ECL emission spectra of (a) PBS buffer (100 mM, pH=7.4) solution containing 0.1 M $K_2S_2O_8$. (b) is (a) + 10 μg/mL GQDs. (c) further addition of 18 nM and (d) 9 nM AuNPs to (b), respectively. (e) addition of 500 nM cp53 to (b). (f) successive addition of 9 nM AuNPs and 500 nM cp53 without previous coupling. (g) changing the cp53 concentration of 250 nM in (f).

Control experiments were carried out by addition of AuNPs without coupling of capturing DNA, capturing DNA without linked with AuNPs, AuNPs and capturing DNA without coupled together, respectively. No ECL intensity decrease was observed for above mentioned situations (Figure 4B). Thus, it could concluded that the ECL quenching of GQDs was due to the strong interaction between GQDs and capturing DNA, which brought AuNPs close to GQDs and occurrence of ERET.

In addition, the ECL intensity of the GQDs decreased with the increasing amount of AuNPs-ssDNA, which trended to a minimum value after 9 nM of AuNPs-ssDNA was added to 10 μg/mL GQDs suspension containing 0.1 M $K_2S_2O_8$ (Figure 4A).

Therefore, 0.1 M pH=7.4 PBS buffer containing 9 nM AuNPs-ssDNA+ 10 μg/mL GQDs + 0.1 M $K_2S_2O_8$ was chosen as the detection solution for the following use.

3.3 Application in detection of DNA and DNA damage.

3.3.1 ECL analysis of target p53 DNA.

When AuNPs-ssDNA was hybridized with target p53 ssDNA to form AuNPs-dsDNA, the non-covalent interaction between GQDs and ds-DNA weakened due to lessen of the surface charge of DNA molecules and exposure of the base. Thus the ECL signal of GQDs recovered. The difference between the quenching efficiencies (ECL intensity ratio $(I_0-I)/I_0$, I_0 was the ECL intensity in the absence of AuNPs-ssDNA, I was the ECL intensity in the presence of 9 nM AuNPs-ssDNA and different amount of target p53 ssDNA) of AuNPs-ssDNA and AuNPs-dsDNA to GQDs engendered a method for detection of target p53 DNA. As shown in Figure 5A, the quenching efficiency had induced with the increasing of target p53 sequence concentration with a linear calibration in the range from 25 to 400 nM (inset in Figure 5A). The detection limit for target p53 ssDNA was 13 nM at 3 times of signal-to-noise. These results suggested that the approach of AuNPs quenching GQDs ECL signal was potentially appropriate for quantification of nucleic acid.

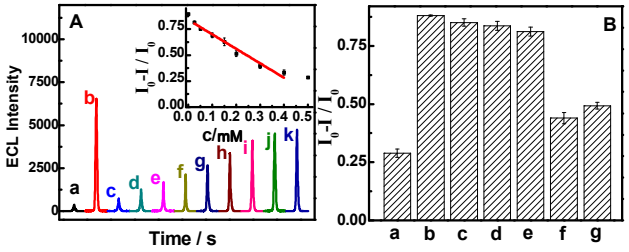

Figure 5. (A) ECL emission spectra in 0.1 M pH 7.4 PBS containing 0.1 M $K_2S_2O_8$ (a) and 10 μg/mL GQDs (b) after addition of 9 nM AuNPs-ssDNA and 0, 0.025, 0.05, 0.1, 0.15, 0.2, 0.3, 0.4, 0.5 μM (c-j) of p53. Inset: plots of ECL intensity ratio upon p53 concentrations. (B) ECL quenching efficient in 0.1 M pH 7.4 PBS containing 0.1 M $K_2S_2O_8$, 10 μg/mL GQDs, 9 nM AuNPs-ssDNA (a) and 500 nM of p53 (b), TNF-α (c), MUC1 aptamer (d) z-DNA (e) SNP p53 (f), TNP p53 (g).

The specificity of the approach was studied using other five kinds of DNA sequences, including TNF-α, MUC1 aptamer, zDNA, single-base mismatch p53 DNA and three-base mismatch p53 DNA. ECL intensity for single-base mismatch sequence was 74.8% of that for the target p53 ssDNA, while the response to the other DNA was 11.3-5.0% of that for the target p53 ssDNA, which was close to the blank control (Figure 5B). Therefore, the approach exhibited good performance to distinguish the target p53 ssDNA, the other DNA and the mismatched stand. This manifested that the suggested system could detect effectively the target with high specificity and had potential application in single nucleotide polymorphism analysis.

3.3.2 Application of ERET in detection of DNA damage.

To detect of DNA damaging, the target p53 ssDNA was first treated with different chemicals, and then hybridized with AuNPs-ssDNA. The damaged nucleobases led DNA to partly unwind or alteration in DNA sequence. This made the damaged target p53 ssDNA with chemicals could not hybridize completely with the cp53 ssDNA on AuNPs to form a fully double helix structure. This changed the surface charge of the dsDNA molecules compared with that of a fully double helix structure and reduced the ECL signal.

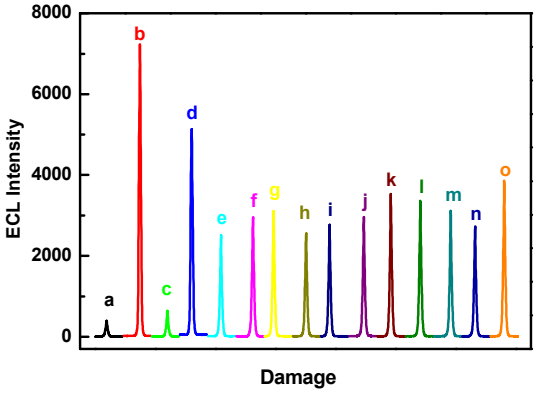

Figure 6. ECL emission spectra in 0.1 M pH 7.4 PBS containing 0.1 M $K_2S_2O_8$ (a) 10 μg/mL GQDs (b) and 9 nM AuNPs-ssDNA (c) after addition of 0.5 μM p53 without damage (d) and with SO, PGA, MA, sodium arsenite, toluene, ether, acetone, methanal, ethanal, methanol and ethanol (e-o) damaged for 1 h.

Figure 6 showed the ECL emission spectra of the GQDs where the target p53 DNA was pretreated by SO, PGA, MA, sodium arsenite, toluene, ether, acetone, methanal, ethanal, methanol and ethanol, respectively. It was observed that the different chemicals had possibly led to the different damage effects or damaging machanism with various chemicals. Therefore, the present strategy could be developed to detect DNA damaging, to classify the damaging machanism with chemicals and to estimate the toxic effect of chemicals.

4. Conclusion

In summary, a bright blue luminescent graphene quantum dots with a PL quantum yield as 15.5% was prepared by thermal reduction coupled with UV-light irradiation. The as-prepared GQDs displayed strong and stable ECL behavior. The non-covalent interaction between cp53 ssDNA and GQDs made the cp53 ssDNA linked AuNPs close to GQDs, which led to occurrence of the electrochemiluminescence resonance energy transfer between GQDs and AuNPs and thus quenched the ECL signal of GQDs. When AuNPs-ssDNA was hybridized with target p53 DNA to form AuNPs-dsDNA, the non-covalent interaction between GQDs and ds-DNA weakened due to lessen of the surface charge of DNA molecules and exposure of the base, which led the ECL of GQDs to be recovered. Therefore, the difference between the quenching efficiencies of AuNPs-ssDNA and AuNPs-dsDNA to GQDs engendered a method for detection of target DNA with a detection limit of 13 nM target DNA. The resultant ECL sensor could be used for DNA damaging detection based on the different bonding ability between damaged target p53 ssDNA to cp53 ssDNA linked AuNPs. The discovery of the electrochemiluminescence resonance energy transfer between graphene quantum dots and gold nanoparticles could be expanded in the development of other ECL biosensors for quantification of nucleic, single nucleotide polymorphism or other aptamer-specific biomolecules.

Acknowledgements

The work is supported by the National Basic Research Program of China (No. 2010CB732400), Key Program (21035002) from the National Natural Science Foundation of China, National Natural Science Foundation of China (Grant Nos. 21175021, 21205014), Natural Science Foundation of Jiangsu province (BK2012734), Open Foundation from Key Laboratory of Environmental Medicine Engineering, Ministry of Education, China.

Notes and references

[a] *Key Laboratory of Environmental Medicine Engineering, Ministry of Education, School of Chemistry and Chemical Engineering, Southeast University, Jiangning District 211189, Nanjing, Jiangsu Province, PR China*

[b] *Second Hospital of Nanjing, 210 014 Nanjing, PR China*

1 K. Zhang, L. L. Zhang, X. S. Zhao and J. S. Wu, *Chem. Mate.,* 2010, **22**, 1392-1401.
2 L. Qu, Y. Liu, J. B. Baek and L. Dai, *Acs Nano,* 2010, **4**, 1321-1326.
3 R. H. Yang, J. Y. Jin, Y. Chen, N. Shao, H. Z. Kang, Z. Xiao, Z. W. Tang, Y. R. Wu, Z. Zhu and W. H. Tan, *J. Am. Chem. Soc.,* 2008, **130**, 8351-8358.
4 W. Cheng, L. Ding, J. Lei, S. Ding and H. Ju, *Anal. Chem.,* 2008, **80**, 3867-3872.
5 S. J. Zhen, L. Q. Chen, S. J. Xiao, Y. F. Li, P. P. Hu, L. Zhan, L. Peng, E. Q. Song and C. Z. Huang, *Anal. Chem.,* 2010, **82**, 8432-8437.
6 L. Matlock-Colangelo and A. J. Baeumner, *Lab Chip,* 2012, **12**, 2612-2620.
7 J. Zhang, P. Loya, C. Peng, V. Khabashesku and J. Lou, *Adv. Funct. Mater.,* 2012, **22**, 4070-4077.
8 C. Hao, L. Ding, X. Zhang and H. Ju, *Anal. Chem.,* 2007, **79**, 4442-4447.
9 B. L. Allen, C. M. Shade, A. M. Yingling and S. Petoud, *Adv. Mater.,* 2009, **21**, 4692-4695.
10 B. L. Allen, M. B. Keddie and A. Star, *Nanoscale,* 2010, **2**, 1105-1108.
11 G. Eda, Y. Y. Lin, C. Mattevi, H. Yamaguchi, H. A. Chen, I. S. Chen, C. W. Chen and M. Chhowalla, *Adv. Mater.,* 2010, **22**, 505-509.
12 K. S. Novoselov, Z. Jiang, Y. Zhang, S. V. Morozov, H. L. Stormer, U. Zeitler, J. C. Maan, G. S. Boebinger, P. Kim and A. K. Geim, *Science,* 2007, **315**, 1379-1379.
13 K. S. Novoselov, A. K. Geim, S. V. Morozov, D. Jiang, M. I. Katsnelson, I. V. Grigorieva, S. V. Dubonos and A. A. Firsov, *Nature,* 2005, **438**, 197-200.
14 X. Li, X. Wang, L. Zhang, S. Lee and H. Dai, *Science,* 2008, **319**, 1229-1232.
15 D. Pan, J. Zhang, Z. Li and M. Wu, *Adv. Mater.,* 2010, **22**, 734-738.
16 Y. Li, Y. Hu, Y. Zhao, G. Shi, L. Deng, Y. Hou and L. Qu, *Adv. Mater.,* 2011, **23**, 776-780.
17 L. L. Li, J. Ji, R. Fei, C. Z. Wang, Q. Lu, J. R. Zhang, L. P. Jiang and J. J. Zhu, *Adv. Funct. Mater.,* 2012, **22**, 2971-2979.
18 S. Zhu, J. Zhang, C. Qiao, S. Tang, Y. Li, W. Yuan, B. Li, L. Tian, F. Liu, R. Hu, H. Gao, H. Wei, H. Zhang, H. Sun and B. Yang, *Chem. Commun.,* 2011, **47**, 6858-6860.
19 S. Neubeck, L. A. Ponomarenko, F. Freitag, A. J. Giesbers, U. Zeitler, S. V. Morozov, P. Blake, A. K. Geim and K. S. Novoselov, *Small,* 2010, **6**, 1469-1473.
20 S. Zhu, J. Zhang, S. Tang, C. Qiao, L. Wang, H. Wang, X. Liu, B. Li, Y. Li, W. Yu, X. Wang, H. Sun and B. Yang, *Adv. Funct. Mater.,* 2012, **22**, 4732-4740.
21 J. Peng, W. Gao, B. K. Gupta, Z. Liu, R. Romero-Aburto, L. Ge, L. Song, L. B. Alemany, X. Zhan, G. Gao, S. A. Vithayathil, B. A. Kaipparettu, A. A. Marti, T. Hayashi, J. J. Zhu and P. M. Ajayan, *Nano. Lett.,* 2012, **12**, 844-849.
22 K. A. Ritter and J. W. Lyding, *Nat. Mater.,* 2009, **8**, 235-242.
23 X. Zhou, Y. Zhang, C. Wang, X. Wu, Y. Yang, B. Zheng, H. Wu, S. Guo and J. Zhang, *Acs Nano,* 2012, **6** , 6592-6599.
24 X. Sun, Z. Liu, K. Welsher, J. T. Robinson, A. Goodwin, S. Zaric and H. Dai, *Nano. Res.,* 2008, **1**, 203-212.
25 X. Yan, X. Cui and L.S. Li, *J. Am. Chem. Soc.,* 2010, **132**, 5944-5945.
26 X. Yan, X. Cui, B. Li and L. S. Li, *Nano. Lett.* **2010**, *10*, 1869-1873.
27 J. Liu and Y. Lu, *Nat. Protoc.,* 2006, **1**, 246-252.
28 J. J. Storhoff, R. Elghanian, R. C. Mucic, C. A. Mirkin and R. L. Letsinger, *J. Am. Chem. Soc.,* 1998, **120**, 1959-1964.
29 H. Y. Shi, L. Yuan, Y. F. Wu and S. Q. Liu, *Biosens. Bioelectron.* 2011, **26**, 3788-3793.
30 R. Elghanian, J. J. Storhoff, R. C. Mucic, R. L. Letsinger and C. A. Mirkin, *Science* 1997, **277**, 1078 -1081.
31 T. H. Ji, Y. Y. Hua, M. Sun and N. Ma, *Carbon,* 2013, **54**, 412-419.
32 M. H. Huang, X. Xu, H. Yang and S. Q. Liu, *RSC Adv.,* 2012, **2**, 12844-12850.
33 J. Qian, C. Wang, X. H. Pan and S. Q. Liu, *Anal. Chim. Acta* 2013, **763**, 43-49.
34 T. Kuila, S. Bose, A. K. Mishra, P. Khanra, N. H. Kim and J. H. Lee, *Prog. Mater. Sci.,* 2012, **57**, 1061-1105.
35 K. S. Novoselov, A. K. Geim, S. V. Morozov, D. Jiang, Y. Zhang, S. V. Dubonos, I. V. Grigorieva and A. A. Firsov, *Science,* 2004, **306**, 666-669.
36 Y. Bae, N. Myung and A. J. Bard, *Nano. Lett.,* 2004, **4**, 1153-1161.
37 N. Myung, Y. Bae and A. J. Bard, *Nano. Lett.,* 2003, **3**, 1053-1055.
38 L. L. Li, K. P. Liu, G. H. Yang, C. M. Wang, J. R. Zhang and J. J. Zhu, *Adv. Funct. Mater.,* 2011, **21**, 869-878.
39 Y. Q. Dong, N. N. Zhou, X. M. Lin, J. P. Lin, Y. W. Chi and G. N. Chen, *Chem. Mater.,* 2010, **22**, 5895-5899.
40 L. Zheng, Y. Chi, Y. Dong, J. Lin and B. Wang, *J. Am. Chem. Soc.,* 2009, **131**, 4564-4565.
41 F. R. F. Fan, S. Park, Y. Zhu, R. S. Ruoff and A. J. Bard, *J. Am. Chem. Soc.,* 2009, **131**, 937-939.
42 Z. Ding, B. M. Quinn, S. K. Haram, L. E. Pell, B. A. Korgel and A. J. Bard, *Science,* 2002, **296**, 1293-1297.
43 H. Y. Han, Z. G. Sheng and J. G. Liang, *Anal. Chim. Acta.,* 2007, **596**, 73-78.
44 J. Qian, C. Zhang, X. D. Cao and S. Q. Liu, *Anal. Chem.,* 2010, **82**, 6422-6429.
45 H. F. Dong, W. C. Gao, F. Yan, H. Ji and H. X. Ju, *Anal. Chem.,* 2010, **82**, 5511-5517.
46 E. Oh, M. Y. Hong, D. Lee, S. H. Nam, H. C. Yoon and H. S. Kim, *J. Am. Chem. Soc.,* 2005, **127**, 3270-3271.
47 X. Liu, H. Jiang, J. P. Lei and H. X. Ju, *Anal. Chem.,* 2007, **79**, 8055-8060.
48 X. Liu, L. Cheng, J. P. Lei and H. X. Ju, *Analyst,* 2008, **133**, 1161-1163.

For AOC

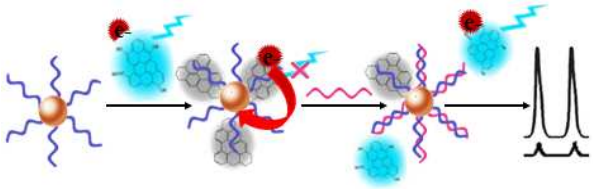

ERET between GQDs and AuNPs results the ECL signal of GQDs quenching or recovering.